Kinetics-dominated interdiffusion in metallic glass-forming liquids

F. Yang,[1,*] P. Heintzmann,[1] F. Kargl,[1] K. Binder,[1] B. Nowak,[1] B. Schillinger,[2] Th. Voigtmann,[1,3] and A. Meyer[1]

[1]*Institut für Materialphysik im Weltraum, Deutsches Zentrum für Luft- und Raumfahrt (DLR), 51170 Köln, Germany*

[2]*Heinz Maier-Leibnitz Zentrum (MLZ) and Physics Department, Technische Universität München, Lichtenbergstr. 1, 85748 Garching, Germany*

[3]*Physics Department, Heinrich-Heine-Universität Düsseldorf, 40225 Düsseldorf, Germany*

(Received 13 February 2017; published 6 August 2018)

With a full set of experimentally obtained self- and interdiffusion coefficients, we are able to verify the relation between different transport coefficients in binary glass-forming Zr-Ni liquids. Despite a thermodynamic strong tendency of mixing, the interdiffusion is up to a factor of 2 slower than that predicted by the Darken equation. With the help of mode-coupling theory calculations, we identify that this is due to a slow, dominating kinetic contribution, arising from the dense packing of the melt, and the coupling of dynamics due to the strong Zr-Ni affinity. As a consequence, the cross correlation is on the order of 0.5 or less, whose contribution cannot be neglected, which seems to be a general feature of the glass-forming melts.

DOI: 10.1103/PhysRevB.98.064202

I. INTRODUCTION

Diffusion is a transport process involving random motion of atoms/molecules [1]. It is one of the key mechanisms controlling a vast number of kinetic processes in liquids and solids, and therefore a very vibrant research topic in physics, chemistry, and material sciences [2,3]. In particular, this includes for liquids: thermal and electric conductivity of ionic melts, adhesion properties of polymers, as well as nucleation and growth of crystalline phases in glass-forming liquids, and hence the stability of the undercooled melt against crystallization [4–8].

According to their driving force diffusion can be divided into self- and chemical (inter-) diffusion. Self-diffusion describes the long range transport of a tagged particle, driven by kinetics, and hence predominantly entropy. Chemical diffusion is driven by the difference in chemical potentials, corresponding to the decay of concentration gradients at large scales [9]. It is obvious that self- and interdiffusion are intimately connected, as both reflect to some extent the atomic mobility of the system. The interdiffusion coefficient can be decomposed into the product of a thermodynamic factor φ and a kinetic coefficient L (Onsager coefficient). For binary systems, applying a very common empirical rule, the so called Darken relation, the kinetic contribution can be expressed by a linear combination of the two self-diffusion coefficients D_A and D_B:

$$D_{\text{int}}^{\text{Darken}} = \varphi L = \varphi(c_{\text{A}} D_{\text{B}} + c_{\text{B}} D_{\text{A}}), \tag{1}$$

whereby c_i are the concentrations of the respective elements A and B [10]. It has been derived from solid diffusion in metals, but is widely applied to liquids and solids/glasses of metallic, ceramic, and molecular materials [6,7].

Despite its broad applications, the Darken relation remains an empirical approximation which assumes ideal mixing behavior and no mixing-induced occurrence of free volume. Microscopically, the thermodynamic factor can be derived from the concentration-concentration partial structure factor at its hydrodynamic limit, while the kinetic coefficient can be expressed by a time integral over an auto-correlation function of the relative velocities of the species [11,12], given by

$$D_{\text{int}} = \varphi[(c_{\text{A}} D_{\text{B}} + c_{\text{B}} D_{\text{A}}) + \Delta_{\text{d}}]. \tag{2}$$

The additional contribution, not taken into account in the Darken relation

$$\Delta_{\text{d}} = c_{\text{A}} c_{\text{B}} \int_0^\infty [\mathbf{\Lambda}_{\text{AA}}(t) + \mathbf{\Lambda}_{\text{BB}}(t) - 2\mathbf{\Lambda}_{\text{AB}}(t)]dt, \tag{3}$$

arises from dynamic cross correlations, where $\mathbf{\Lambda}_{\alpha\beta}(t)$ denotes distinct velocity correlation functions [12]

$$\mathbf{\Lambda}_{\alpha\beta}(t) = \frac{1}{3Nc_\alpha c_\beta} \sum_{k=1}^{N_\alpha} \sum_{\substack{l=1 \\ l\neq k \text{ if } \alpha=\beta}}^{N_\beta} \left\langle \mathbf{v}_k^\alpha(t) \cdot \mathbf{v}_l^\beta(0) \right\rangle. \tag{4}$$

In crystalline solids, in many cases there are well understood diffusion mechanisms [2], and the contribution of the cross correlation Δ_{d} can be taken into account by assuming a vacancy diffusion mechanism, introducing a correction term called Manning factor S [13]

$$S = D_{\text{int}}/[\varphi(c_{\text{A}} D_{\text{B}} + c_{\text{B}} D_{\text{A}})]. \tag{5}$$

In liquids, however, such vacancy diffusion mechanism is absent due to the disordered nature. While S can be used to quantify the deviation from Darken equation, its physical meaning is unclear and can be only derived if experimental data are available. Therefore, although interdiffusion is a fundamental property, the mechanism in liquids which governs this mass transport processes is still poorly understood. This is also largely due to the lack of reliable experimental data, since the measurement of diffusion coefficients using conventional *ex situ* long-capillary (LC) methods is often hampered by artifacts from convection, chemical reaction, and uncertainties

*fan.yang@dlr.de

in the diffusion times and length caused by melting and solidification [14].

In situ diagnostics significantly improves the accuracy of the diffusion measurements, which has been applied for optically transparent melts, even in space missions [4,5]. For metallic melts, *in situ* measurements have been realized only recently, employing x-ray and neutron radiography [15–19]. Using radiography and quasielastic neutron scattering (QNS), it is now possible to measure diffusion coefficients in metallic liquids precisely on an absolute scale [20]. So far, *in situ* interdiffusion studies focused mainly on Al-based liquid alloys, since they provide an excellent x-ray radiographic contrast [15–19]. For metallic glass-forming liquids, experimental studies of the interdiffusion coefficient has been performed, e.g., on PdNiCuP alloys, using shear-cell technique and *ex situ* analysis [21]. However, a large part of these melts are multicomponent alloys and often chemically reactive. Thus, systematic studies are rare and have not been carried out *in situ* up to now.

Here we report results of *in situ* radiography measurements on binary glass-forming Zr-Ni alloys of the compositions $Zr_{64}Ni_{36}$ and $Zr_{36}Ni_{64}$, in order to understand the contribution of kinetics and thermodynamics to interdiffusion in dense metallic melts. Unlike the Al-based alloys, glass-forming metallic melts are usually characterized by: (1) a more dense packing, (2) asymmetry in the atomic size of their constituents, and (3) very often a large negative mixing enthalpy, hence a large thermodynamic driving force of mixing [22].

The Zr-Ni system was chosen since the Ni self-diffusion coefficients and the viscosity of binary $Zr_{64}Ni_{36}$ melt are similar compared to those of the Zr-based multicomponent bulk metallic glass-forming (BMG) alloys. Hence, it can be considered as a model system for studying the liquid dynamics of these BMGs [23,24]. Zr and Ni self-diffusion coefficients and partial structure factors in Zr-Ni alloys have been measured. Also computer simulation data as well as experimentally determined partial structure factors are available [23–30]. This allows a comprehensive comparison between experimental and simulation results to understand the transport mechanism. Zr and Ni exhibit a large negative enthalpy of mixing, indicating a preferred formation of Zr-Ni pairs. A large φ is reported from thermodynamic assessment [31]. However, we show that the interdiffusion in these alloys is in fact dominated by a slow kinetic contribution.

II. METHOD

A. Radiography

For the *in situ* radiography measurements in $Zr_{64}Ni_{36}$ and $Zr_{36}Ni_{64}$ alloys, diffusion couples with the composition of $Zr_{66.7}Ni_{33.3} - Zr_{60}Ni_{40}$ and $Zr_{32}Ni_{68} - Zr_{42}Ni_{58}$ were prepared, respectively. The compositions were chosen such that while concentration differences are kept at a minimum, sufficient radiography contrast is still obtained. This ensures that in the data analysis a concentration independent diffusion coefficient can be reasonably assumed. Moreover, the liquidus temperatures of these compositions are similar. This minimizes the influence of perturbations during melting of the alloys on the diffusion process. Master ingots (∼1 g) were prepared for each composition by alloying of proper amounts of Zr

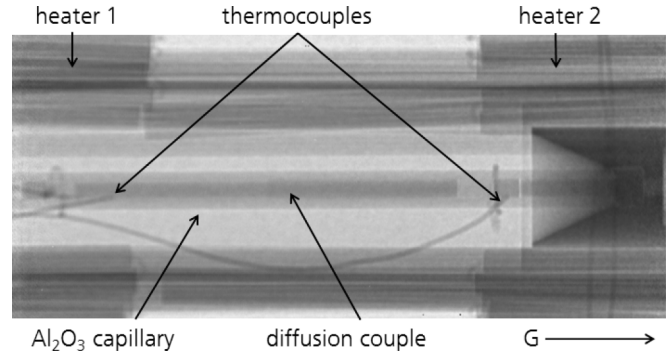

FIG. 1. A neutron radiographic image of the long capillary furnace setup with a diffusion couple taken at ANTARES at the FRM II. G indicates the direction of the gravity.

(smart-element®, 99.97%) and Ni (Alfa Aesar®, 99.995%) in a compact arc-melter (MAM-1, Edmund Bühler®) under a Ti-gettered pure Ar atmosphere (99.9999%). Rods of 1.5 mm in diameter and 12–15 mm in length were then prepared for the diffusion experiments by suction casting the arc-melted liquid alloy into a copper mold and checked to be homogeneous and free of shrinkage holes.

To obtain sufficient contrast in the experiments neutron radiography (NR) was used for Zr-rich samples and x-ray radiography (XRR) for Ni-rich samples, respectively. The reason is that in NR Ni exhibits a higher absorbance compared that of Zr, while the opposite holds in XRR. The experiments were carried out in a previously described long-capillary furnace optimized for neutron radiography [15]. Figure 1 shows a radiographic image of the furnace for illustration purposes. The axial temperature gradient for a 25 mm long diffusion couple is less than 2 K at the experimental temperatures, verified using a dummy sample with the same assembly. In XRR experiments the alumina capillary containing the sample was additionally surrounded by a graphite tube, which further improves the temperature homogeneity to be better than 1 K axially over the entire sample length. The vacuum in the furnace was better than 1×10^{-3} mbar during the entire experiment.

NR experiments on $Zr_{60}Ni_{40} - Zr_{66.7}Ni_{33.3}$ diffusion couples have been performed at 1423 K and 1503 K on the cold neutron radiography station ANTARES (Advanced Neutron Tomography And Radiography Experimental System) at FRM II (Forschungs-Neutronenquelle Heinz Maier-Leibnitz). XRR experiments on $Zr_{32}Ni_{68} - Zr_{42}Ni_{58}$ diffusion couples were performed at 1453 K, 1483 K, and 1503 K using the x-ray setup described in Ref. [17]. The spatial resolution was about 70 μm per pixel for NR and 35 μm per pixel for XRR. Radiographic images were taken at 10 s time intervals for NR and 5 s time intervals for XRR, respectively. In an experiment the diffusion couple is fully molten and then annealed at a given target temperature. Typically the capillary was preheated to temperatures slightly below the lowest solidus temperature of the present compositions ($Zr_{60}Ni_{40} - Zr_{66.7}Ni_{33.3}$: 1273 K; $Zr_{32}Ni_{68} - Zr_{42}Ni_{58}$ 1333 K). From there the target diffusion temperature was reached with a heating rate of about 50 K/min. During melting the diffusion couple length decreased due to complete filling of the capillary. This is assisted by pushing of an Al_2O_3 rod against the sample surface using a spring mechanism. This ensures that the whole sample surface is

in contact with the Al_2O_3 capillary wall, which suppresses Marangoni flow. Buoyancy convection is not detectable, suppressed by stable density layering of the diffusion couple, achieved by placing the less dense alloy on top of the denser alloy.

From the grayscale in the recorded radiographic image, the space and time dependent concentration profile $c(z,t)$ can be calculated using the Lambert-Beer's law [32]. It is assumed that the number density of the atoms in the sample and the optical path length through the sample are constant along the entire sample. These assumptions are reasonable considering the sample density [24] and their relatively short length, as well as a fairly small beam divergence. In NR the beam is almost parallel. In XRR the source-sample distance (~450 mm) is also much large compared to the sample length (max. 30 mm), giving a divergence angle of about 1.9°.

The squared time dependent diffusion length $l^2 = 4D_{\text{int}}t$ can be obtained via a fit of an error function to the data

$$c(z,t) = \frac{c_1 + c_2}{2} + \frac{c_1 - c_2}{2}\text{erf}\left(\frac{z - z_0}{l}\right), \qquad (6)$$

where z_0 is the center of the diffusion couple, z is the position along the sample axis, c_1 and c_2 are the initial composition at either end of the diffusion couple, and D_{int} is the interdiffusion coefficient. The function is a solution of Fick's second law of diffusion for an infinitely long, one-dimensional diffusion couple [33].

B. Mode-coupling theory calculation

Model-coupling theory allows (MCT) prediction of dynamics of dense liquids by solving the equation of motion provided according to Zwanzig-Mori formalism for density correlation function $\Phi_q(t) = \langle \rho_q(t)^* \rho_q \rangle / S(q)$

$$\ddot{\Phi}_q(t) + \Omega_q^2 \Phi_q(t) + \int_0^t M_q(t-t')\dot{\Phi}_q(t')dt' = 0, \qquad (7)$$

where Ω_q corresponds to thermal velocities which govern the short-time relaxation (phonon), and $M_q(t)$ is the so-called memory kernel which is a nonlinear functional of the density correlation function [34]. Kinetic quantities like the self-diffusion coefficient and the Onsager coefficient L can be derived by the corresponding Green-Kubo integrals of the self- and distinct velocity auto-correlation functions, respectively, by solving the equation of motion using the (static) partial structure factors $S(q)$ that enter $\Phi_q(t)$ as input.

MCT predicts full arrest at a critical temperature T_c. Around and below T_c, additional relaxation modes become important but are neglected by the theory. For this reason, MCT does not predict the dynamics on an absolute scale without adjustable parameters. But this is a systematic error that, above T_c, affects all mass transport coefficients equally. Hence, inter- and self-diffusion coefficients obtained in a single calculation can be compared. The ratio between them is even comparable to experimental results. More importantly however, we focus here on the differences between results obtained using different liquid structure factors, since MCT allows the prediction of dynamics directly from the liquid structures. This allows specific structural features in the melt to be associated to the dynamics.

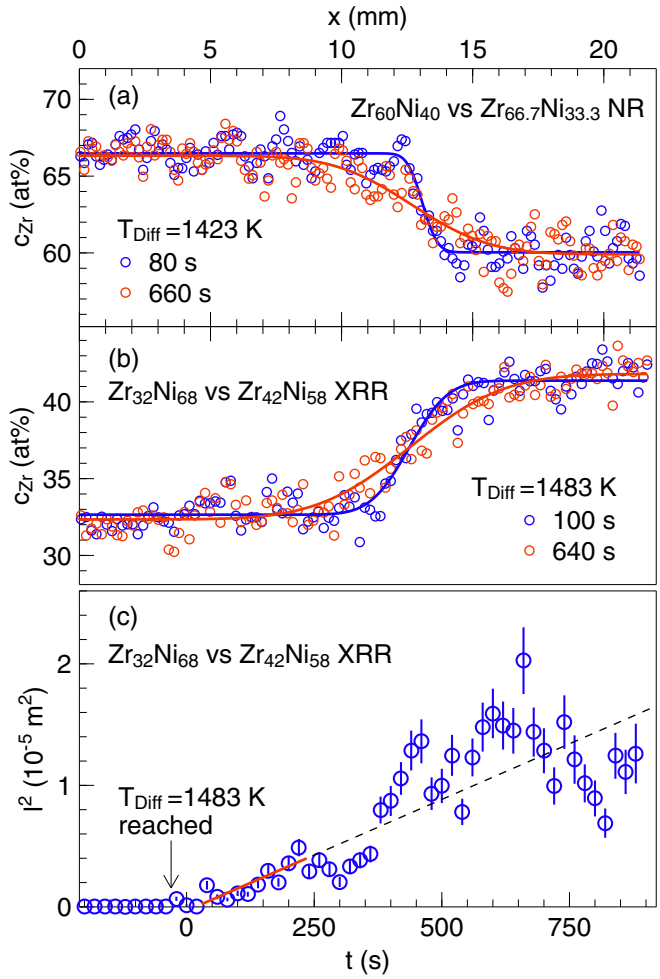

FIG. 2. Derived concentration profile of (a) a $Zr_{32}Ni_{68} - Zr_{42}Ni_{58}$ and (b) a $Zr_{66.7}Ni_{33.3} - Zr_{60}Ni_{40}$ diffusion couple at different times during the experiment. (c) Time evolution of the mean square displacement measured on the $Zr_{32}Ni_{68} - Zr_{42}Ni_{58}$ diffusion couple. Red solid line: linear fit between 30 s and 230 s; black dashed line: extrapolation of the fit. The error bar in (c) represents only the uncertainty of the l^2 from the fitting procedure.

For this purpose MCT calculations have been performed on two sets of different liquid partial structure factors: experimentally determined partial structure factors of $Zr_{64}Ni_{36}$, $Zr_{50}Ni_{50}$, and $Zr_{36}Ni_{64}$ alloy melts [30], and partial structure factors of the corresponding binary hard-sphere (HS) like mixtures. The structure factors of the HS mixtures are approximated by the Percus-Yevick (PY) equation [9], with a size ratio of $r_{large}/r_{small} = 1.26$ between the two components, in order to mimic the size ratio between Zr ($r_{Zr} = 1.45$ Å) and Ni ($r_{Ni} = 1.15$ Å) atoms. Compared to the Zr-Ni melt, HS mixtures exhibit ideal mixing behavior, which allows us to disentangle the impact of the chemical short range order.

III. RESULTS

Figures 2(a) and 2(b) show the measured concentration profiles together with the error function fits for NR and XRR, respectively. Figure 2(c) shows the resulting time dependent l^2 for the diffusion couple $Zr_{32}Ni_{68} - Zr_{42}Ni_{58}$ measured

with XRR, evaluated by averaging every two images. $t = 0$ is defined as the time when the sample length stopped to change, usually an indication of complete melting. The target temperature in the case of Fig. 2(c) was reached at about $t = -30$ s. However, there are still a significant portion of solid phase before the liquidus temperature is reached, and the viscosity of the melt is relatively high. Thus, there is almost no broadening from a step function that occurs before $t = 20$ s. Between 30 s and 230 s, l^2 follows a linear time dependence from which D_{int} is obtained. If this would be analyzed *ex situ*, this would correspond to an average of 9–10 diffusion profiles all at different diffusion times. In addition, the time during melting can be excluded for evaluating the D_{int}, demonstrating again the advantage of the *in situ* method. After 250 s, the scattering in l^2 becomes larger, although its time dependence still appears to follow overall the determined linear scaling. The larger scattering is due to the reduction of the radiography contrast with progressing diffusion.

For $Zr_{36}Ni_{64}$ the interdiffusion coefficient measured by XRR is $3.9 \pm 0.7 \times 10^{-9}$ m^{2}s^{-1} at 1453 K, $4.4 \pm 1.0 \times 10^{-9}$ m^2 s^{-1} at 1483 K, and $5.1 \pm 1.0 \times 10^{-9}$ m^2 s^{-1} at 1503 K, respectively. For $Zr_{64}Ni_{36}$ the interdiffusion coefficient at 1503 K was measured to be $2.9 \pm 0.9 \times 10^{-9}$ m^2 s^{-1}. For 1423 K it decreases to $1.7 \pm 0.5 \times 10^{-9}$ m^2 s^{-1}, which is an average over three independent measurements. The uncertainty in D_{int} amounts to about 20% in XRR and about 30% in NR due to the larger statistical noise.

For Zr-Ni melts self-diffusion coefficients of both Zr and Ni have been reported in the literature, determined experimentally using either QNS (Ni) or radiotracer (Co,Zr) methods [23,29,35]. In the radiotracer experiment the measurement on the Co tracer is considered to represent the diffusion behavior of Ni. These self-diffusion coefficients for both $Zr_{64}Ni_{36}$ and $Zr_{36}Ni_{64}$ are shown in Fig. 3 together with the here determined interdiffusion coefficients. Also diffusion coefficients obtained from MD simulations and from MCT calculations at temperatures where partial structure factors are measured are displayed [28,29].

The interdiffusion coefficient in $Zr_{64}Ni_{36}$ (mean value of three data points) is a factor of 1.5 ± 0.2 larger than the self-diffusion coefficient of Ni at 1423 K. This factor increases slightly to 1.9 ± 0.6 at 1503 K. For $Zr_{36}Ni_{64}$ the ratios between the interdiffusion and Ni self-diffusion coefficients is 4.4 ± 0.3 at 1453 K and 4.8 ± 1.4 at 1503 K, respectively. This is at first glance not surprising since Zr and Ni exhibit a large, negative enthalpy of mixing, and thermodynamic driving force contributes to the interdiffusion.

The interdiffusion coefficient obtained from MD simulations performed on a model of liquid Zr-Ni alloys using an embedded atom potential exhibit a similar trend: Interdiffusion is faster than the self diffusion for both compositions studied [29]. However, as visible in Fig. 3, quantitatively the simulated interdiffusion coefficient for $Zr_{64}Ni_{36}$ is up to a factor two larger than the experimental values reported here. For the $Zr_{36}Ni_{64}$ melt the discrepancy between simulation and experiment is of about 50%. It seems that the embedded atom potential used is not precise enough to model interdiffusion quantitatively, despite the fact that it has been optimized to accurately reproduce Ni self diffusion in both $Zr_{64}Ni_{36}$ and $Zr_{36}Ni_{64}$ melts.

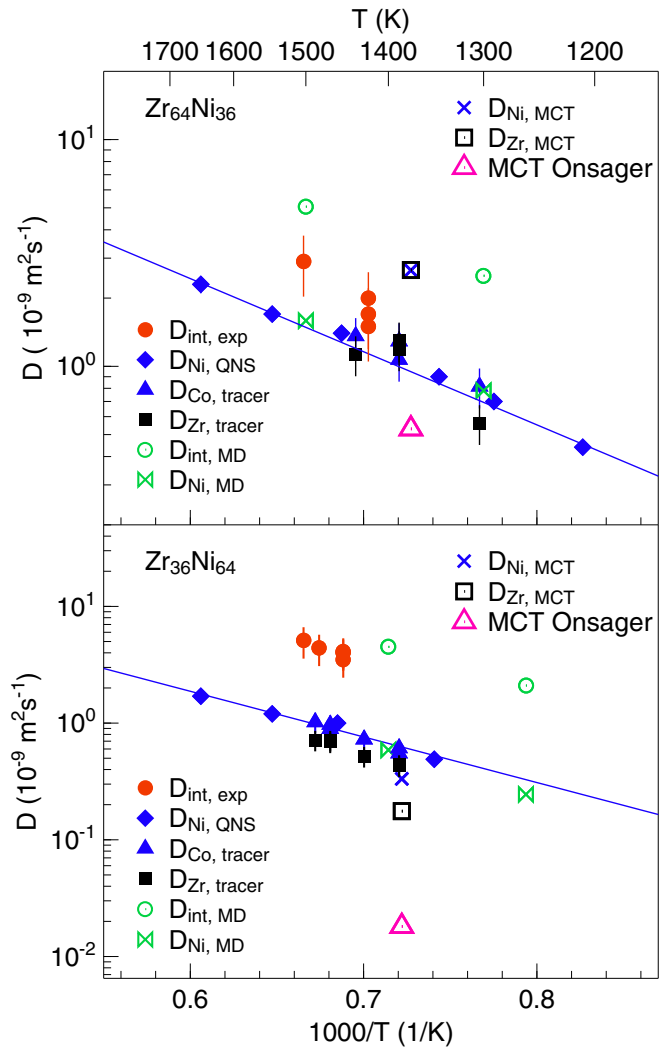

FIG. 3. Temperature dependent self- and interdiffusion coefficients in $Zr_{64}Ni_{36}$ (upper panel) and $Zr_{36}Ni_{64}$ melts. Interdiffusion coefficients are measured with NR. Self-diffusion coefficients of Ni/Co and Zr are determined by QNS and radiotracer techniques [23,35]. Besides the experimental data also data from MD simulations and MCT calculations [28,29] are shown. Full symbols represent experimental measured data, and open symbols represent simulation/calculation.

It can be seen in Fig. 3 that the MCT calculations based on the measured partial structure factors of the Zr-Ni melts underestimate the transport coefficients on absolute scale. However, compared to the experimental results, the relative ratio between the self-diffusion coefficients of Zr and Ni is well reproduced. Moreover, it can be seen that the Onsager coefficient, i.e., the kinetic contribution, directly accessible from the MCT calculation, is even smaller than the self-diffusion coefficients for both alloys. This is not expected according to the Darken equation, which will be discussed in more details together with the composition dependence.

Figure 4 shows the obtained transport coefficients from MCT calculation for three different compositions $Zr_{36}Ni_{64}$, $Zr_{50}Ni_{50}$, and $Zr_{64}Ni_{36}$ at 1385 K, 1445 K, and 1375 K, respectively, where (partial) structure factors were measured

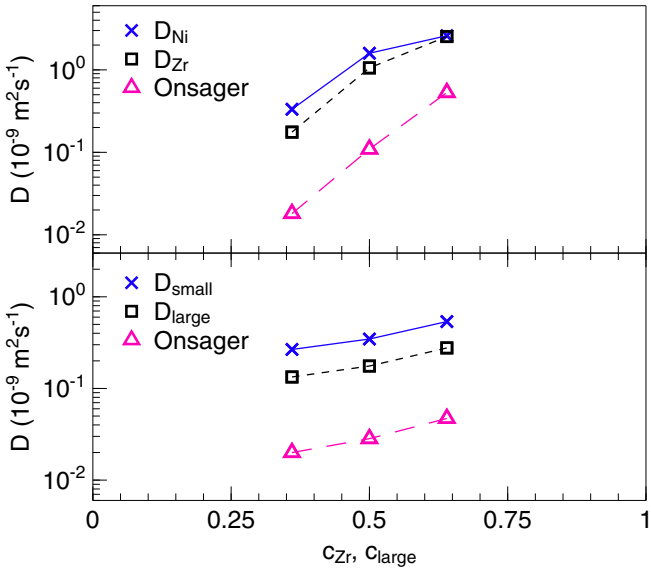

FIG. 4. Self-diffusion coefficient and Onsager coefficients calculated by MCT using (upper panel) measured partial structure factors of $Zr_{36}Ni_{64}$, $Zr_{50}Ni_{50}$, $Zr_{64}Ni_{36}$ melts and using (lower panel) PY approximated partial structure factors of the corresponding HS mixtures.

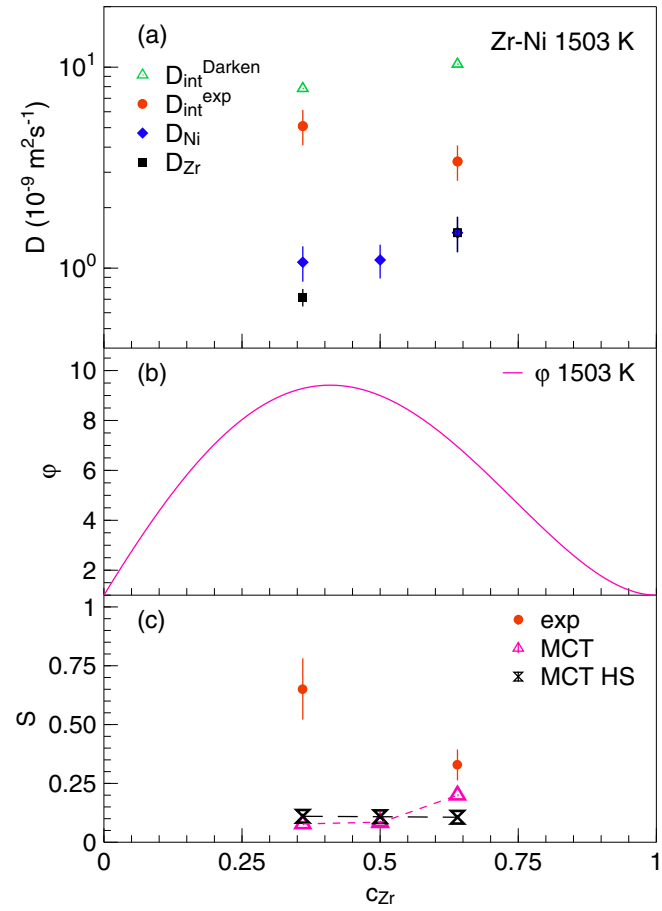

FIG. 5. (a) Composition dependence of the self- and interdiffusion coefficients in the binary Zr-Ni melts at 1503 K (closed symbols) [23,35]. The open triangles represent values expected by the Darken equation. (b) Thermodynamic factor φ from Ghosh's thermodynamic assessment [31]. (c) Cross-correlation S derived from experimental data and from MCT calculations; both show that the Darken equation overestimates the D_{int} using the measured self-diffusion coefficients.

experimentally [30]. The corresponding calculations of the binary HS mixtures were performed at a density close to the density of the alloy at the liquidus temperature ($0.9\rho_l$). Compared to the Zr-Ni MCT results, in the HS mixture, $D_{\text{large}}/D_{\text{small}}$ is closed to the ratio of experimental measured self-diffusion values at the small atom (Ni) rich side, but does not decrease to $\sim$1 as that for the Zr-rich composition. This can be understood by the preferred formation of Zr-Ni pairs and hence the coupled diffusion towards the Zr-rich side of the alloy system [30].

On the other hand, for both Zr-Ni melts and HS mixtures, the Onsager coefficient is considerably smaller. In the Zr-Ni melts, the calculated Ni self-diffusion coefficient is almost an order of magnitude faster compared to the calculated Onsager coefficient for $Zr_{36}Ni_{64}$, which decreases to a factor of 5 for $Zr_{64}Ni_{36}$. For the binary HS mixtures studied, the ratio between the self-diffusion coefficient of the small spheres and the Onsager coefficient is almost composition independent, which remains at about a factor of 10.

IV. DISCUSSION

Figure 5(a) compares the experimental measured self- and interdiffusion coefficients with the interdiffusion coefficient predicted by the Darken equation $D_{\text{int}}^{\text{Darken}}$ using a thermodynamic factor derived from Ghosh's thermodynamic assessment of the alloys [31]. For both Zr-Ni liquids reported here, the Darken relation overestimates the interdiffusion coefficient. The deviation increases with increasing Zr content, on the Zr-rich side even by more than a factor of 2.

This is qualitatively in agreement with the small kinetic contribution observed in the MCT calculation, viewed at best by calculating the cross-correlation term S, as shown in Fig. 5(c). From the measured self- and interdiffusion coefficient, the cross-correlation term can be derived according to Eq. (5). For the diffusion coefficients obtained in MCT calculation, S can be directly obtained by $L/(c_{\text{Zr}}D_{\text{Ni}} + c_{\text{Ni}}D_{\text{Zr}})$, independent of the thermodynamic factor φ. If one consider that $D_{\text{int}} = \varphi L$, and S represents solely the deviation of the kinetic contribution from the linear combination of the self-diffusion coefficients. It can be seen that both the experimental data and the MCT calculation give $S < 1$, which confirms that Darken equation overestimates the interdiffusion coefficient. The experimental obtained S at 1503 K is about 0.33 ± 0.08 for $Zr_{64}Ni_{36}$ and 0.65 ± 0.15 for $Zr_{36}Ni_{64}$, respectively. In the MCT calculation not only for Zr-Ni melts, but also for HS-like mixture where chemical short-range order (CSRO) is negligible the S is on the order of 0.1.

Thus, all these results show consistently that the Darken equation overestimates the interdiffusion coefficient. We would like to emphasize that the S obtained can be only compared on a qualitative level. On the one hand, the error given in the S derived from experimentally measured diffusion coefficient represents only the uncertainty of the diffusion data. The uncertainty of the thermodynamic factor is not known. It

is also not necessarily small considering that φ is a second derivative of the thermodynamic functions, and the fact that due to the high chemical reactivity of the Zr-Ni alloys thermophysical data are rare [31]. On the other hand, systematic errors are present in the S obtained from MCT calculation, since the temperature does not necessarily correspond to that at which the self- and interdiffusion coefficient is measured, although the temperature dependence of the ratio between the diffusion coefficients is small. Nevertheless, despite the difference in the absolute values of S, it is obvious that the kinetic contribution dominates the interdiffusion coefficients and is slower compared to that expected from the Darken equation.

Deviations from the Darken equation in crystalline materials usually indicate a nonideal mixing behavior. However, it seems that in the investigated composition range large deviations of the interdiffusion coefficient can be found even for the HS like mixtures, which should show an ideal mixing behavior. This indicates that the transport mechanism in the melt is completely different compared to that in the crystalline solids. The possibility to separately study the impact of geometric packing and that of the CSRO in the MCT calculation allows us now to reveal more details of the the underlying mechanism. Obviously for the HS mixtures such deviation has to arise from effects similar to steric hindrance, where the dense packing of the melt plays an important role.

In addition, it is known that the interdiffusion is also lower than expected by the Darken relation for melts like Al-Ni or ionic liquids, which exhibit a strong affinity between the components [11,12,18], and the diffusion species are strongly coupled [5]. In these cases the kinetic term is also smaller than the self diffusion coefficients, which can be understood by the fact that microscopically the decay of the velocity correlation of the unequal species $\mathbf{\Lambda}_{\mathrm{AB}}(t)$ is slower than that of the equal ones $\mathbf{\Lambda}_{\mathrm{AA}}(t)$ and $\mathbf{\Lambda}_{\mathrm{BB}}(t)$, resulting in a negative dynamic cross-correlation contribution Δ_{d} [11,12], and $S < 1$. Therefore, also CSRO and the formation of preferred heterogeneous pairs contribute to the slow kinetics of the interdiffusion.

Metallic glass-forming alloys are typically densely packed, and most of them also exhibit a pronounced CSRO [36]. Although the strong affinity between the alloy components like that in Zr-Ni leads to large thermodynamic factor, it only raises the interdiffusion coefficient to a scale similar to the self-diffusion, due to a slow, dominating kinetic contribution [16–19]. Thus, the composition and temperature dependent interdiffusion behavior is much more complicated than expressed by the Darken relation.

V. CONCLUSION

In summary, combining different radiography techniques, we were able to determine accurately the interdiffusion coefficient of the glass-forming Zr-Ni melts. With a full set of experimentally determined self- and interdiffusion coefficients, we show that in the Zr-Ni alloy melts the interdiffusion is dominated by a slow kinetic contribution, despite the large thermodynamic driving force of mixing. Darken equation overestimates the interdiffusion, indicating that the contribution of the dynamic cross correlations cannot be neglected. Particularly, utilizing MCT calculation, and comparing to a hard-sphere-like mixture, we are able to show that the contribution of the cross correlation mainly arises from the dense packing of the melt. This could be a general feature of these metallic glass formers, where a sluggish interdiffusion impedes crystal growth and facilitates glass formation.

ACKNOWLEDGMENTS

We thank E. Calzada for the technical support during the experiment at FRM II, and E. Sondermann for a careful reading of the manuscript. The financial support provided by the Deutsche Forschungsgemeinschaft (DFG) through the Grant (No. ME 1958/10-1) is gratefully acknowledged.

[1] A. Einstein, Ann. d. Phys. **17**, 549 (1905).
[2] H. Mehrer, *Diffusion in Solids: Fundamentals, Methods, Materials, Diffusion-Controlled Processes*, Springer Series in Solid-State Sciences (Springer, Berlin, Heidelberg, 2007).
[3] E. Cussler, *Diffusion: Mass Transfer in Fluid Systems*, Cambridge Series in Chemical Engineering (Cambridge University Press, Cambridge, 2009).
[4] J. Richter, A. Leuchter, and N. Großer, J. Mol. Liq. **103**, 359 (2003).
[5] J. Bert and J. Dupuy-Philon, J. Phys.: Condens. Matter **9**, 11045 (1997).
[6] A. F. Copper and J. H. Heasley, J. Am. Ceram. Soc. **49**, 280 (1966).
[7] E. J. Kramer, P. Green, and C. J. Palmstrøm, Polymer **25**, 473 (1984).
[8] D. M. Herlach, P. Galenko, and D. Holland-Moritz, eds., *Metastable solids from undercooled melts* (Pergamon, Oxford, 2007).
[9] J. P. Hansen and I. R. McDonald, *Theory of simple liquids* (Academic Press, London, 1986).
[10] L. S. Darken, Trans. AIME **175**, 184 (1948).
[11] M. Schoen and C. Hoheisel, Mol. Phys. **53**, 1367 (1984).
[12] J. Horbach, S. K. Das, A. Griesche, M.-P. Macht, G. Frohberg, and A. Meyer, Phys. Rev. B **75**, 174304 (2007).
[13] J. R. Manning, Phys. Rev. **116**, 69 (1959).
[14] A. Griesche, M.-P. Macht, and G. Frohberg, J. Non-Cryst. Solids **353**, 3305 (2007), liquid and Amorphous Metals XII.
[15] F. Kargl, M. Engelhardt, F. Yang, H. Weis, P. Schmakat, B. Schillinger, A. Griesche, and A. Meyer, J. Phys.: Condens. Matter **23**, 254201 (2011).
[16] B. Zhang, A. Griesche, and A. Meyer, Phys. Rev. Lett. **104**, 035902 (2010).
[17] F. Kargl, E. Sondermann, H. Weis, and A. Meyer, HTHP **42**, 3 (2013).
[18] E. Sondermann, F. Kargl, and A. Meyer, Phys. Rev. B **93**, 184201 (2016).

[19] M. Engelhardt, A. Meyer, F. Yang, G. G. Simeoni, and F. Kargl, Def. Diff. Forum **367**, 157 (2016).
[20] A. Meyer and F. Kargl, Int. J. Microgravity Sci. Appl. **30**, 30 (2013).
[21] A. Griesche, M.-P. Macht, and G. Frohberg, Scr. Mater. **53**, 1395 (2005).
[22] A. Inoue and A. Takeuchi, Mater. Trans., JIM **43**, 1892 (2002).
[23] T. Kordel, D. Holland-Moritz, F. Yang, J. Peters, T. Unruh, T. Hansen, and A. Meyer, Phys. Rev. B **83**, 104205 (2011).
[24] P. Heintzmann, F. Yang, S. Schneider, G. Lohöfer, and A. Meyer, Appl. Phys. Lett. **108**, 241908 (2016).
[25] D. Holland-Moritz, S. Stüber, H. Hartmann, T. Unruh, T. Hansen, and A. Meyer, Phys. Rev. B **79**, 064204 (2009).
[26] D. Holland-Moritz, S. Stüber, H. Hartmann, T. Unruh, and A. Meyer, J. Phys.: Conf. Series **144**, 012119 (2009).
[27] J. Brillo, A. I. Pommrich, and A. Meyer, Phys. Rev. Lett. **107**, 165902 (2011).
[28] T. Voigtmann, A. Meyer, D. Holland-Moritz, S. Stüber, T. Hansen, and T. Unruh, Europhys. Lett. **82**, 66001 (2008).
[29] P. Kuhn, J. Horbach, F. Kargl, A. Meyer, and T. Voigtmann, Phys. Rev. B **90**, 024309 (2014).
[30] B. Nowak, D. Holland-Moritz, F. Yang, T. Voigtmann, T. Kordel, T. C. Hansen, and A. Meyer, Phys. Rev. Materials **1**, 025603 (2017).
[31] G. Ghosh, J. Mater. Res. **9**, 598 (1994).
[32] A. Beer, Ann. d. Phys. **162**, 78 (1852).
[33] J. Crank, *The Mathematics of Diffusion*, 2nd ed. (Oxford University Press, Oxford, 1975).
[34] W. Götze and L. Sjögren, Rep. Prog. Phys. **55**, 241 (1992).
[35] S. W. Basuki, F. Yang, E. Gill, K. Rätzke, A. Meyer, and F. Faupel, Phys. Rev. B **95**, 024301 (2017).
[36] J. Brillo, *Thermophysical Properties of Multicomponent Liquid Alloys* (De Gruyter, Berlin, 2016).